

Search for new physics via single top production at TeV energy $e\gamma$ colliders

Qing-Hong Cao* and Jose Wudka†

Physics Department, University of California Riverside, Riverside, CA 92521, USA

(Dated: October 14, 2018)

Abstract

We study the sensitivity of $e\gamma$ colliders to physics beyond the Standard Model, when such interactions are natural and their scale lies below the collider energy. Using the reaction $e\gamma \rightarrow bt\nu$ as a specific example, we show that the deviations from the Standard Model can be parameterized in a model independent way by only 3 numbers. We investigate the sensitivity of several observables to these 3 quantities, using the various collider polarization modes to increase the signal to noise ratio. These results are then translated into the expected sensitivity derived from this reaction to the new physics effects present in several specific models.

*Electronic address: qcao@ucr.edu

†Electronic address: jose.wudka@ucr.edu

I. INTRODUCTION

The top quark is by far the heaviest known fermion with a mass at the electroweak symmetry breaking scale. Assuming this is not a coincidence, it is hoped that a detailed study of top quark couplings to other particles will be of utility in clarifying whether the Standard Model (SM) provides the correct mechanism for electroweak symmetry-breaking, or whether new physics is responsible.

It is therefore of interest to provide a general description of the top-quark couplings, which might be modified due to the presence of new interactions and/or particles. In this paper we will assume that such new effects are indeed present, but that the energies available at present and near-future colliders lie below their typical new-physics scale Λ . In this case the characteristics of the new interactions can be probed only through their virtual effects on processes involving SM particles; such effects can be efficiently coded in a model-independent way using the well-studied effective-Lagrangian formalism [1, 2, 3].

The search for deviations from the SM couplings in single top production has become one of the main focus in the forthcoming experiments at the Large Hadron Collider (LHC) and the various Linear Collider (LC) proposals. For example, the sensitivity to non-standard Wtb couplings at the LHC via the single top quark production has been studied in several papers [4, 5, 6, 7, 8, 9, 10, 11]. It has also been shown [12] that a very high energy LC with 500 fb^{-1} luminosity will eventually improve the LHC limits by a factor of 3-8, depending on the coupling under consideration.

Future linear colliders are expected to be designed to function also as $e\gamma$ and $\gamma\gamma$ colliders through Compton back-scattering of laser light off one or both lepton beams [13]; in these modes the flexibility in polarizing both lepton and photon beams will allow unique opportunities to analyze the top quark properties and interactions. This is illustrated in [14, 15] for the case of the Wtb coupling; and in [16] for that of the four-Fermi operators in $e^+e^- \rightarrow t\bar{t}$ and top-quark decay.

It is generally the case that a given process receives contributions from a variety of new-physics effects which are difficult to disentangle. We will show that an exception to this is provided by single-top production in an $e\gamma$ collider. We argue that in natural theories new physics effects for this process can be parameterized by only three quantities, and we will provide observables that can be used to measure them independently

This paper is organized as follows. In Sec. II, we list the dominating new-physics contributions to the single-top production in $e\gamma$ collisions and summarize the existing experimental constraints on the corresponding coefficients. In Sect. III we analyze the effects of the non-SM coefficients in the distribution of several observables as function of the beam energy and polarization parameters. These results are then used to study the sensibility of this reaction to the effects predicted by several models (Sect. IV). Conclusions and parting comments are presented in Sect. V.

II. FRAMEWORK

In this section, we summarize the basic elements of the framework used in the analysis (additional details are included in the appendices).

A. Effective Lagrangian

The arguments suggesting the existence of physics beyond the SM and the uses of the effective Lagrangian approach (ELA) for describing these new interactions have been extensively discussed [1, 2, 3]. In the ELA it is assumed that none of the heavy excitations can be directly produced, so that all new physics effects can be parameterized by gauge-invariant operators of dimension higher than four constructed out of the SM fields. These higher-order operators are suppressed by inverse powers of the new physics scale Λ (the scale at which the excitations of the underlying theory can be directly probed). Among the effective operators those of dimension 5 necessarily violate lepton number [17, 18, 19], and are strongly bounded by existing data [20]; the largest contributions are then expected to be generated by dimension-6 operators, which we denote as \mathcal{O}_i . The effective Lagrangian then takes the form ¹

$$\mathcal{L}_{eff} = \mathcal{L}_{SM} + \frac{1}{\Lambda^2} \sum_i (C_i \mathcal{O}_i + \text{H.c.}) + O(\Lambda^{-3}), \quad (1)$$

where C_i are coefficients that parametrize the non-standard interactions. Some of the \mathcal{O}_i can be generated by tree graphs in the underlying theory, while other are necessarily loop-

¹ It is worth mentioning that the effects of some tree-level induced dimension-8 operators may compete with those from dimension-6 operators if the latter are generated at the one-loop level, and thus have associated a suppression factor of $1/(4\pi)^2$.

generated [21] and the corresponding C_i will be suppressed by a numerical factor $\sim 1/16\pi^2$. We will therefore focus our attention on the tree-level induced operators only, and examine their effects in the single top production in $e\gamma$ collisions. These operators fall in two categories: those modifying the Wtb coupling, and those that generate four fermion interactions; we will discuss them separately

There are only 2 tree-level generated operators of the first type:

$$\mathcal{O}_{\phi q}^{(3)} = i (\phi^\dagger \tau^I D_\mu \phi) (\bar{q} \gamma^\mu \tau^I q) + \text{H.c.}, \quad (2)$$

$$\mathcal{O}_{\phi\phi} = i (\phi^\dagger \epsilon D_\mu \phi) (\bar{t} \gamma^\mu b) + \text{H.c.}, \quad (3)$$

where ϕ denotes the SM scalar doublet, D_μ the covariant derivative, $q(\ell)$ the quark (lepton) isodoublets and $t(b)$ the corresponding isosinglets (we follow the notation of [20]). After symmetry breaking, these operators generate the following contribution to the Wtb coupling

$$\mathcal{L}_{Wtb}^{(\text{dim}-6)} = \frac{g}{\sqrt{2}} \{ \bar{t} \gamma^\mu (\mathcal{F}_L P_L + \mathcal{F}_R P_R) b W_\mu^+ + \text{H.c.} \}, \quad (4)$$

with

$$\mathcal{F}_L = \frac{C_{\phi q}^{(3)} v^2}{\Lambda^2}, \quad \mathcal{F}_R = \frac{C_{\phi\phi} v^2}{2\Lambda^2}, \quad (5)$$

where $v = 246$ GeV is the vacuum expectation value (VEV).

There are 4 operators of the second type:

$$\begin{aligned} \mathcal{O}_{qde} &= (\bar{\ell} e) (\bar{b} q), & \mathcal{O}_{\ell q} &= (\bar{\ell} e) \epsilon (\bar{q} t), \\ \mathcal{O}_{\ell q'} &= (\bar{\ell} t) \epsilon (\bar{q} e), & \mathcal{O}_{\ell q}^{(3)} &= \frac{1}{2} (\bar{\ell} \gamma_\mu \tau^I \ell) (\bar{q} \gamma^\mu \tau^I q). \end{aligned} \quad (6)$$

all of which can be generated at tree level [21]. The first three, however, involve a chirality flip; in a natural theory this implies that the corresponding coefficients will be proportional to m_e and can be ignored. Hence, we only need to consider the last operator, $\mathcal{O}_{\ell q}^{(3)}$, from which we extract out the following effective $\ell\nu bt$ vertex:

$$\mathcal{L}_{4f} = \frac{\mathcal{G}_{4f}}{\Lambda^2} \{ (\bar{\nu} \gamma^\mu P_L e) (\bar{b} \gamma_\mu P_L t) + (\bar{e} \gamma^\mu P_L \nu) (\bar{t} \gamma_\mu P_L b) \}, \quad (7)$$

with $\mathcal{G}_{4f} = C_{\ell q}^{(3)}/2$.

In our calculation we will take all the effective couplings to be real in order to simplify our analysis. We will also assume that the $\nu\ell W$ vertex does not receive significant contributions from physics beyond the SM ².

² A rough estimate shows that the scale of new physics that would modify this vertex lies above ~ 7 TeV.

B. Constraints of the effective operators

The LEP precision data requires $|\mathcal{F}_L| \leq 0.02$ [22], assuming no deviations from the SM ttZ vertex. Recent data on $b \rightarrow s\gamma$ provides the limit $|\mathcal{F}_R| < 0.004$ [22, 23, 24], provided one neglects other possible new-physics effects, such as those embodied in a $bstt$ 4-fermion interaction (that could be generated, for example, by a heavy W' vector boson with flavor-changing couplings).

The four-fermion interaction operator will violate the unitarity constraints at high energies; the resulting constraint (see, for example [25]) is

$$|\mathcal{G}_{4f}| < \frac{16\pi}{s}\Lambda^2 < 16\pi. \quad (8)$$

since the ELA is valid only for $\Lambda > s$. We note that even when $\mathcal{G}_{4f} = O(50)$ the 4-fermion operators in Eq. 7 will only affect the branching ratio for $t \rightarrow b\ell\nu_\ell$ at the 0.1% level³, well within the current experimental bound $Br(t \rightarrow b\ell\nu) = 9.4 \pm 2.4\%$ [26]. In contrast the effects of this operator in single top quark production can be very significant. This is because this reaction is dominated by the t -channel processes involving a virtual W^* boson ($q_W^2 < 0$) which receives two kinematic enhancements: (i) the W^* propagator does not suffer the $1/s$ suppression⁴, and (ii) the photon-splitting ($\gamma \rightarrow b\bar{b}$) collinear enhancement. Therefore the interference effects of the SM contribution and the \mathcal{G}_{4f} contribution can be large.

Due to the strong constraint on \mathcal{F}_R (assuming no cancellations with a possible $bstt$ contribution), its effects are negligible. Hence, we will concentrate on the effects of couplings \mathcal{F}_L and \mathcal{G}_{4f} in various kinematics distributions (though, for completeness, we will include some effects generated by \mathcal{F}_R). It is clear, however, that \mathcal{F}_L merely produces a change in the overall normalization of the SM cross-section, so it will be difficult to disentangle its contribution from the SM background unless one can measure the event rate very accurately.

³ This is because the SM contributions to the amplitude peak in the region of phase space where $(p_\ell + p_\nu)^2 \simeq M_W^2$ in which case their interference with the \mathcal{G}_{4f} term can be ignored; the new-physics corrections to the differential decay rate are then $O(1/\Lambda^4)$.

⁴ The invariant mass of the virtual W boson peaks around 200 GeV for $\sqrt{s} = 500$ GeV, and at 300 GeV for $\sqrt{s} = 1$ TeV

TABLE I: The choices of the polarization parameters.

| | \mathcal{P}_e | \mathcal{P}_t | \mathcal{P}_γ | | \mathcal{P}_e | \mathcal{P}_t | \mathcal{P}_γ |
|-----|-----------------|-----------------|----------------------|-----|-----------------|-----------------|----------------------|
| (1) | +1 | 0 | +1 | (5) | +1 | +1 | 0 |
| (2) | -1 | 0 | +1 | (6) | -1 | +1 | 0 |
| (3) | +1 | 0 | -1 | (7) | +1 | $1/\sqrt{2}$ | $1\sqrt{2}$ |
| (4) | -1 | 0 | -1 | (8) | -1 | $1/\sqrt{2}$ | $1/\sqrt{2}$ |

III. PHENOMENOLOGICAL STUDY

The expressions for the cross section and helicity amplitudes for the process of $e\gamma \rightarrow \nu tb$ are given in the appendices. Using these results we examine the sensitivity of this reaction to the effective operators mentioned above, and discuss how beam polarization can be used to optimize this sensitivity.

For the numerical evaluation we choose the following set of SM input parameters: $\alpha = 1/137.0359895$, $G_\mu = 1.16637 \times 10^{-5} \text{ GeV}^{-2}$, $M_W = 80.35 \text{ GeV}$, $\Gamma_W = 2.0887 \text{ GeV}$, $M_Z = 91.1867 \text{ GeV}$, $m_e = 0.51099907 \text{ MeV}$. The square of the weak gauge coupling is then $g^2 = 4\sqrt{2}M_W^2G_\mu$ and the branching ratio of the W boson into leptons is $Br(W \rightarrow \ell^+\nu) = 0.108$ [27] (including the $O(\alpha_s)$ corrections to $W \rightarrow \bar{q}q'$).

At the linear collider it will be possible to adjust the initial-state electron and positron longitudinal-polarizations \mathcal{P}_e and $\mathcal{P}_{\bar{e}}$, the average helicities of the initial-state photons \mathcal{P}_γ and $\mathcal{P}_{\bar{\gamma}}$, and their maximum average linear-polarization \mathcal{P}_t and $\mathcal{P}_{\bar{t}}$ with the azimuthal angles φ and $\tilde{\varphi}$ (we use the same conventions as [13]). In this study we restrict ourselves to the 8 choices shown in Table I. The first (last) 4 sets correspond to circularly (linearly)-polarized initial photons; the spin-density matrix depends on φ only for the last two sets (see Appendix A); for these cases we found that the cross section is maximized when $\varphi \sim 1.18$, so we will use this value for the rest of calculation.

A. Inclusive cross section

In Fig. 1 we show the inclusive cross section of the process $e^+\gamma \rightarrow \bar{\nu}t\bar{b}$ as a function of the beam energy (\sqrt{s}) for the various choices of polarization parameters (PP). We note that the cross section is significantly larger for set (4), which is due to the fact that in this case

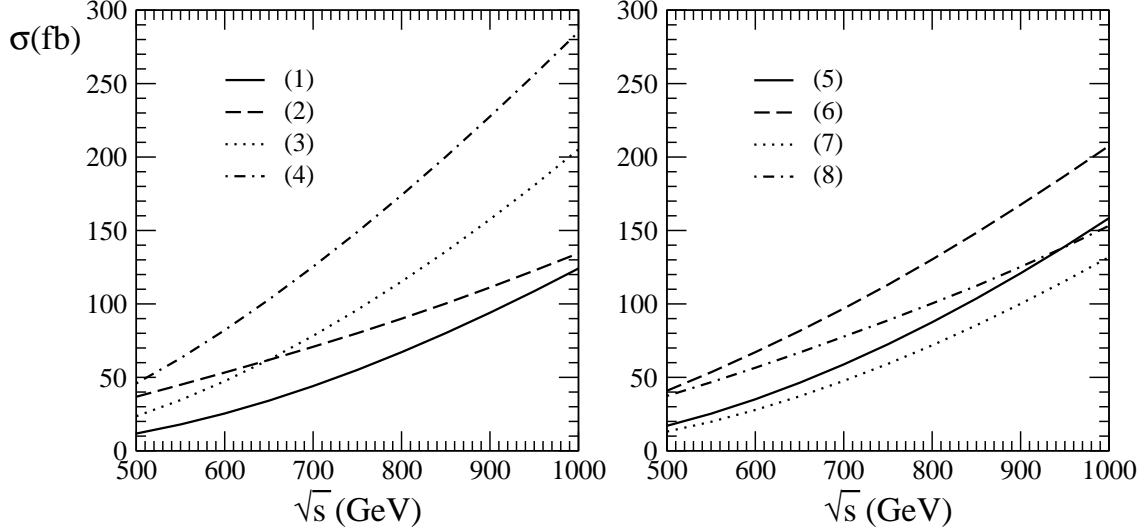


FIG. 1: The inclusive cross section of the process $e^+\gamma \rightarrow \bar{\nu}t\bar{b}$ as a function of the beam energy in the SM. The labels (1-8) denote the choice of polarization parameter set defined in the text.

almost all the scattered photons have negative helicity (see Fig. 8), so their interactions with the right-handed positrons are unsuppressed by factors of the electron mass⁵ [28].

Including the contributions of the effective operators, the cross section takes the following form

$$\begin{aligned}\sigma &= \sigma_{SM} + \sum_i c_i \delta\sigma_i + \dots \\ &= \sigma_{SM} + \mathcal{F}_L \delta\sigma_{\mathcal{F}_L} + \mathcal{F}_R \delta\sigma_{\mathcal{F}_R} + \mathcal{G}'_{4f} \delta\sigma_{\mathcal{G}'_{4f}} + \dots\end{aligned}\quad (9)$$

where

$$\mathcal{G}'_{4f} = \mathcal{G}_{4f} \left(\frac{1\text{TeV}}{\Lambda} \right)^2, \quad (10)$$

σ_{SM} is the SM cross section, and the $\delta\sigma_i$ are the non-standard contributions generated by the effective operators. In this section we will consider one parameter at a time with the other couplings being fixed to the SM values; since we assume $s \ll \Lambda^2$ we can ignore all the terms of order of $1/\Lambda^4$.

The terms containing \mathcal{F}_L are proportional to the SM contributions so $\delta\sigma_{\mathcal{F}_L} = 2\sigma_{SM}$. The remaining $\delta\sigma_i$ are presented in Table II for various choices of polarizations and beam

⁵ In contrast, for set (1) almost all scattered photons will have positive helicity leading to an m_e suppression factor.

TABLE II: The various contributions to the cross section for the reaction $e^+\gamma \rightarrow \bar{\nu}t\bar{b}$ (9) with the various choices of the polarization parameters in table I.

| \sqrt{s} (TeV) | 0.5 | | | | | | | | 1.0 | | | | | | | |
|--|------|------|------|------|------|------|------|------|------|------|------|------|------|------|------|------|
| PP set | (1) | (2) | (3) | (4) | (5) | (6) | (7) | (8) | (1) | (2) | (3) | (4) | (5) | (6) | (7) | (8) |
| $\sigma_{SM}(\text{fb})$ | 23.4 | 73.6 | 47.0 | 91.6 | 34.0 | 81.6 | 26.2 | 74.6 | 248 | 280 | 412 | 570 | 324 | 432 | 270 | 318 |
| $\delta\sigma_{\mathcal{F}_R}/\sigma_{SM}$ | 0.45 | 0.18 | 0.25 | 0.15 | 0.35 | 0.15 | 0.43 | 0.18 | 0.03 | 0.23 | 0.15 | 0.14 | 0.20 | 0.15 | 0.20 | 0.25 |
| $\delta\sigma_{\mathcal{G}'_{4f}}/\sigma_{SM}$ | 0.09 | 0.12 | 0.10 | 0.12 | 0.10 | 0.12 | 0.09 | 0.12 | 0.11 | 0.11 | 0.12 | 0.12 | 0.12 | 0.12 | 0.11 | 0.11 |

energies. We find that $\delta\sigma_{\mathcal{G}'_{4f}} \sim 0.1\sigma_{SM}$ so that a few thousand events should be sufficient to probe \mathcal{G}'_{4f} to $O(1)$

B. Basic kinematic distributions

The relatively large effects observed in the total cross section suggest that other observables might be useful in probing the details of the effective interactions by choosing the PP set that maximizes their significance $\mathcal{S}/\sqrt{\mathcal{B}}$ of the observables under consideration (\mathcal{S} denotes the signal and \mathcal{B} the SM background). Below we follow this procedure for several kinematic variables (in most of the cases we examined the PP set (2) is preferred).

Specifically, given a variable ϕ we expand the differential cross section $d\sigma/d\phi$ in terms of the effective operator coefficients as in (9) and define the normalized distribution functions

$$f_{SM}(\phi) = \frac{1}{\sigma_{SM}} \frac{d\sigma_{SM}}{d\phi}, \quad f_{4f}(\phi) = \frac{1}{\delta\sigma_{\mathcal{G}'_{4f}}} \frac{d\delta\sigma_{\mathcal{G}'_{4f}}}{d\phi}. \quad (11)$$

The values of these quantities, combined with the results of table II, can be used to determine the usefulness of a given choice of ϕ in observing or bounding the magnitude of the new physics effects.

The top quark produced via single-top quark process is highly polarized due to the nature of left- or right-handed charged weak current interaction [29, 30, 31]. Hence a strong spin correlation exists between the final state particles and the initial state leptons. In order to fully understand these correlations, we first examine the ideal case where the back-scattered photon is either left-handed or right-handed polarized. We then study the spin correlation effects with a realistic photon beam. In the last part of this section we examine the effective operators effects in the distribution of several other kinematic variables.

In the following we will choose $+\hat{z}$ as the direction of the incoming photon; we define θ_t , $\theta_{\bar{b}}$ as the polar angles of the t and \bar{b} quarks respectively and denote $\theta_{t\bar{b}}$ as the angle between the directions of the t and \bar{b} quarks

1. *Angular distributions for perfectly polarized photon beams*

For photon energies $\gg m_b$ the final-state \bar{b} quarks move preferentially along the beam line direction due to the collinear enhancement, hence $\cos \theta_{\bar{b}} \simeq 1$ irrespective of the photon polarization. In contrast both $\cos \theta_t$ and $\cos \theta_{t\bar{b}}$ are very sensitive to the polarization of the incoming photon; in order to fully understand the differences between these quantities we examine (Fig. 2) their distributions for purely polarized beams in the center of momentum frame.

Within the SM, left-handed photons ($\lambda_\gamma = -1$) preferentially generate top and \bar{b} quarks moving parallel or anti-parallel to the incoming photons ($\cos \theta_t, \pm \cos \theta_{t\bar{b}} \simeq 1$). In contrast, right-handed photons generate top quarks moving either parallel or anti-parallel to the direction of the incoming photon, with the \bar{b} moving in the opposite direction ($\cos \theta_t, -\cos \theta_{t\bar{b}} \simeq \pm 1$). These distributions remain essentially unchanged when the four-Fermion contribution is included except when $\lambda_\gamma = -1$, in which case the \bar{b} will preferentially move parallel to the t .

The SM results can be explained within the effective- W boson approximation (EWA) [32], that has been used in the study of heavy quark and lepton production [33, 34]. The method is based on the observation that at high energies the W^\pm and Z^0 bosons can be treated as parton constituents of the leptons, in which case a t -channel single top quark event in hadron collisions is dominated by diagrams containing a longitudinal W^* boson [35] since its couplings to the fermions are enhanced by powers of m_t/m_W relative to those of the transversely polarized bosons⁶. For the same reason the SM contributions to the process $e^+\gamma \rightarrow \bar{\nu}t\bar{b}$ are dominated by t -channel-like exchange diagrams Figs. 9(a),(b). The main features of Fig. 2 then follow from angular momentum conservation, see Fig. 3.

⁶ Though the separation into transverse and longitudinal components is not Lorentz invariant, the transverse degrees of freedom remain transverse under boosts in the beam-line direction; though the longitudinal ones mix with the temporal ones, gauge invariance of the physical amplitude for the sub-process insures that the correct result is preserved.

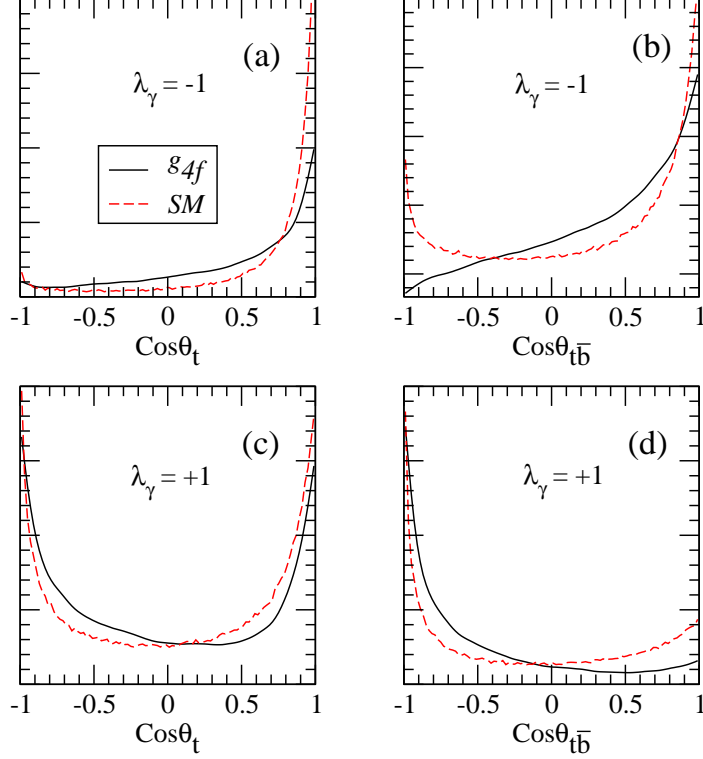


FIG. 2: Normalized distributions (11) for $\phi = \cos \theta_t$ and $\phi = \cos \theta_{t\bar{b}}$ for purely left ($\lambda_\gamma = -1$) and right-handed photons ($\lambda_\gamma = +1$), and $\sqrt{s} = 500$ GeV. Solid curves: f_{4f} ; dashed curves: f_{SM} .

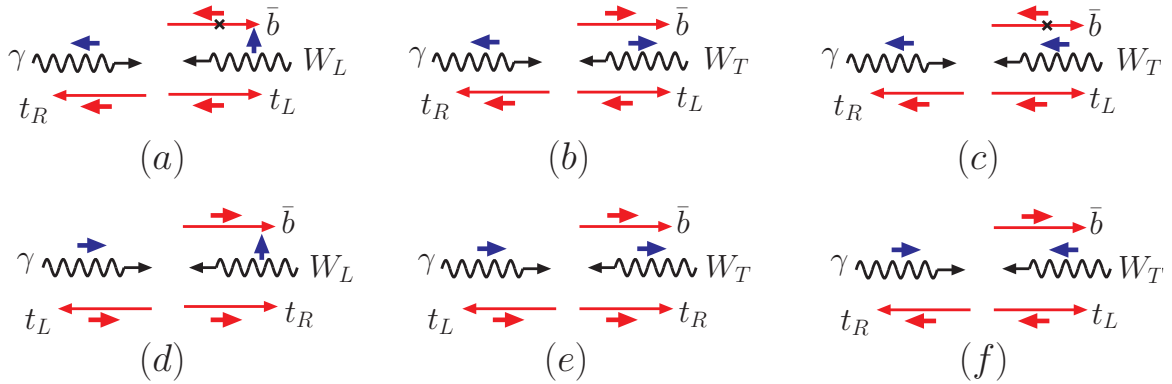


FIG. 3: Kinematic configurations of the t and \bar{b} quarks when both of them move along the beam line. The upper (lower) three plots correspond to left (right)-handed polarized photons. The long straight (waved) lines denote the the direction of motion of the fermions (bosons). The short bold arrows denote the particle's spin direction; a cross on a fermion line indicates a mass insertion, which flips the fermion's helicity.

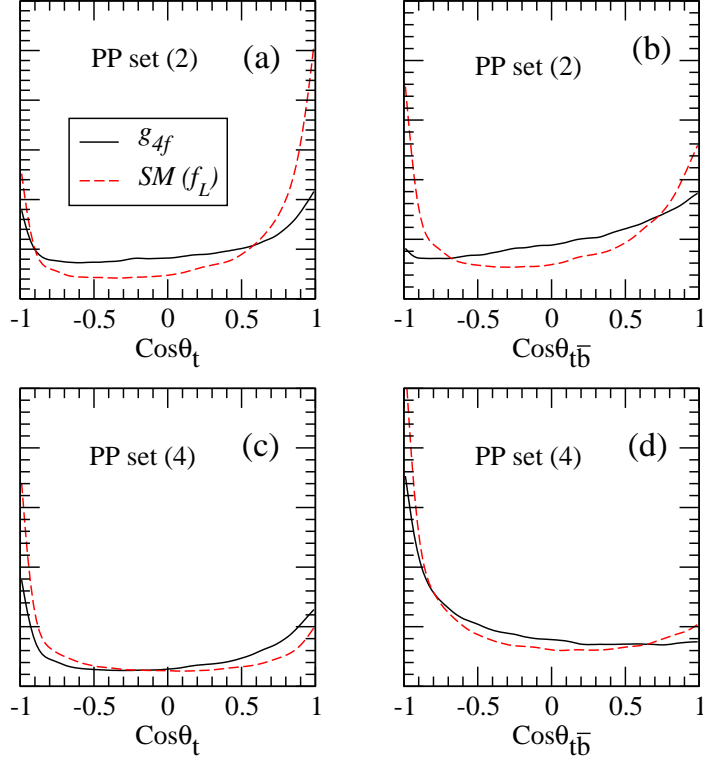


FIG. 4: Same as in fig. 2 for realistic photon beams. Figures (a) and (b) were obtained using the polarization parameter set (2); (c) and (d) using set (4).

These considerations cannot be extended to the case where the 4-fermion operator (Eq. 7) is included since such an operator can be interpreted as being produced by the exchange of a heavy charged W' gauge boson in the underlying theory, whose typical energy lies *below* its mass, so that the EWA approximation cannot be used, and the contribution from the lepton ($e^+\bar{\nu}$) and heavy-quark ($t\bar{b}$) lines cannot be factorized. Nevertheless, since the main deviations from the SM are produced by the interference effects between the SM and the 4-fermion operator, many of the features of the SM are observed in the f_{4f} distributions for $\cos\theta_t$ and $\cos\theta_{t\bar{b}}$.

2. Angular distributions for realistic photon beams.

For photon beams generated through Compton back-scattering, the distributions for θ_t , $\theta_{\bar{b}}$ and $\theta_{t\bar{b}}$ exhibit roughly the same behavior as for the previous ideal case. In particular $\cos\theta_t$ remains sensitive to both the effective operators and initial-state polarization parameters.

In Figs. 4 we show the distributions of $\cos\theta_t$ and $\cos\theta_{t\bar{b}}$ for the PP sets (2) and (4) for

$\sqrt{s} = 500 \text{ GeV}$. From this it is clear that left-handed polarized photons dominate for PP set (2), which is consistent with the photon spectrum distributions in Fig. 8(2). As a result, the SM contribution peaks when the top quark moves along the beam line in the forward direction, while the \mathcal{G}_{4f} contribution shifts the top quark off the beam axis, (Fig. 4(a)). The net contribution of left and right-handed photons results in two peaks in the SM contribution to the $\cos\theta_{t\bar{b}}$ distribution, while the corresponding \mathcal{G}_{4f} contribution is flat (Fig. 4(b)).

The origin of the distributions for PP set (4) is less direct. Though the spectrum of the left-handed polarized photon dominates over the one of right-handed photon (Fig. 8(4)), the sub-process amplitudes of the right-handed photon are enhanced by the contribution of the longitudinal polarized W boson. The distributions in Fig. 4(c) and (d) result from a combination of these effects.

3. Missing energy

Figs. 5(a) and (b) show the normalized distributions (Eq. 11) for the missing energy (E_T) carried by the final-state neutrino. Within the SM the neutrino comes from the initial state positron after emitting a W boson, so its transverse momentum peaks at $\sim M_W/2$. The \mathcal{G}_{4f} contribution tends to shift the missing energy to the large transverse momentum region, which can be understood if we assume the four-Fermi operator is induced by a heavy W' boson: due to the large W' mass, the neutrino produced by a virtual W' boson will have a larger p_T .

4. Rapidity of the bottom quark

Fig. 6 shows the rapidity distribution of the bottom quark. Since the bottom quark is predominately produced from the initial state photon splitting, (Fig. 9(b)), its rapidity peaks in the forward direction, (dashed curves in Fig. 6). The $WW\gamma$ diagram (Fig. 9(d)) corresponds to a virtual W boson moving in the negative rapidity region, balancing the $\bar{\nu}$ emitted from the incoming e^+ . This virtual W boson has a large invariant mass and it is produced mainly in the central rapidity region; its decay products, the \bar{b} and t quarks, also populate this region, which leads to the small kink in the $\eta_{\bar{b}} \sim -1$ region. The \mathcal{G}_{4f} contribution slightly shifts the bottom quark distributions towards the central region where

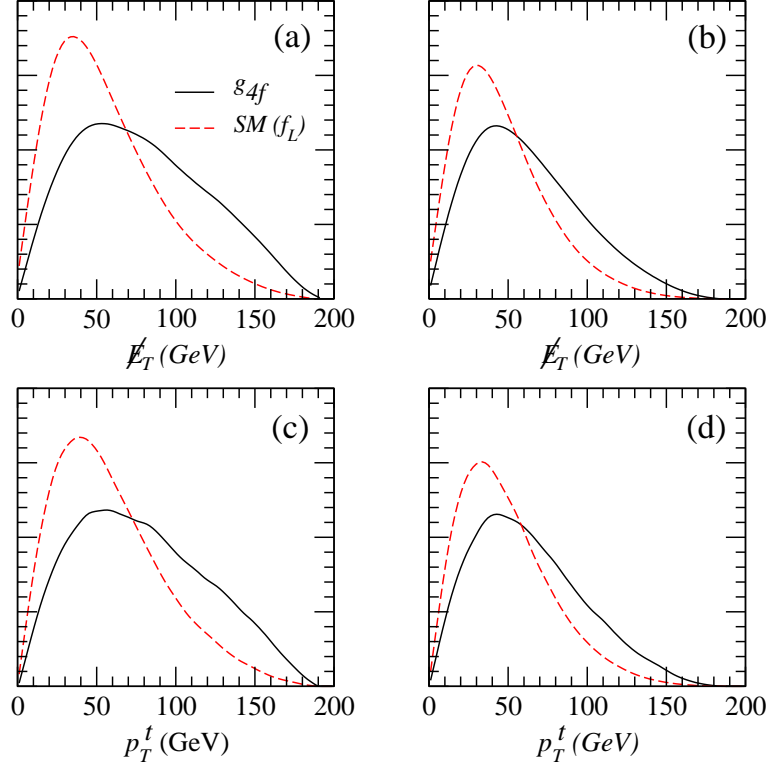


FIG. 5: Normalized distributions (11) f_{SM} (dashed curves) and f_{4f} (solid curves) for the missing energy (\cancel{E}_T) and the top-quark transverse momentum (p_T^t), for $\sqrt{s} = 500$ GeV. (a) and (c) PP set 2, (b) and (d) PP set 4.

it generates a negative peak. This reduces the SM kink at $\eta_{\bar{b}} \sim -1$ and enhances the peak in the forward region.

IV. PHENOMENOLOGICAL CONSEQUENCES.

In this section we discuss the accuracy with which effective couplings \mathcal{F}_L and \mathcal{G}_{4f} can be measured in the reaction $e^+\gamma \rightarrow \bar{\nu}t\bar{b}$ process for beam energies of $\sqrt{s} = 500$ GeV and 1 TeV. Using these results we will discuss the extent to which various models can be differentiated.

The behavior observed in figure 5 suggests that that a cut on the missing energy or transverse top-quark momentum, p_T^t , $\cancel{E}_T \geq 60$ GeV will suppress the SM contribution and allow an accurate measure the effective coupling \mathcal{G}_{4f} . Using the results of tables II and III together with (Eq. 10) and (Eq. 11) we find that with a luminosity of 100 fb^{-1} the four-femrion interaction will produce more than a 3-standard deviation effect for $\mathcal{G}'_{4f} > 0.3$; the

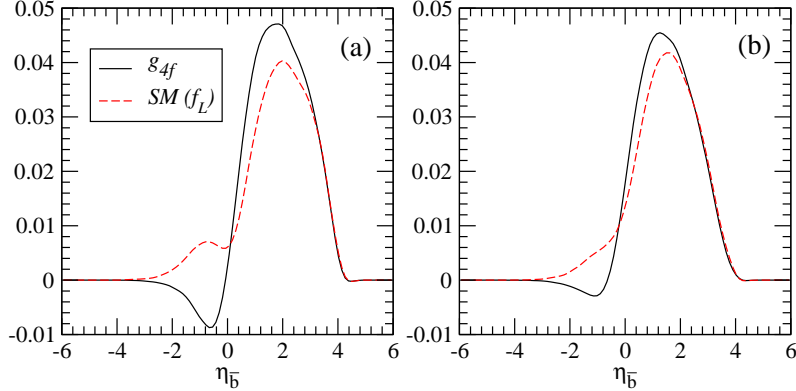


FIG. 6: The normalized distribution of the rapidity of the anti-bottom quark for $\sqrt{s} = 500$ GeV: (a) PP set (2), (b) PP set (4). The red dashed curves denote the SM contributions; solid black curves correspond to the interference of the \mathcal{G}_{4f} and SM graphs .

TABLE III: Integrated distribution functions for the neutrino missing energy and top-quark transverse momentum with $\sqrt{s} = 500$ GeV

| PP | ϕ | $\int_{60}^{\infty} d\phi f_{4f}(\phi)$ | $\int_{60}^{\infty} d\phi f_{SM}(\phi)$ |
|------|---------|---|---|
| 2 | E_T | 0.62 | 0.38 |
| | p_T^t | 0.63 | 0.42 |
| 4 | E_T | 0.47 | 0.28 |
| | p_T^t | 0.49 | 0.31 |

corresponding numbers for 500 fb^{-1} and 1000 fb^{-1} are $\mathcal{G}'_{4f} > 0.13$ and $\mathcal{G}'_{4f} > 0.09$ respectively. These results might be modified by possible correlations with \mathcal{F}_L , \mathcal{F}_R ; in order to include these effects we performed an optimal-observable analysis, to which we now turn.

A. Optimal observable analysis

The optimal observable technique is a useful tool for estimating expected statistical uncertainties in various coupling measurements. Suppose we obtain a differential cross section in terms of some convenient kinematic variables ϕ ,

$$\Sigma(\phi) = \frac{d\sigma}{d\phi} = \sum_i c_i f_i(\phi) \quad (12)$$

TABLE IV: The minimal statistical errors $\overline{\Delta c_i}$ ($c_i = \mathcal{F}_L, \mathcal{F}_R, \mathcal{G}_{4f}$) for various energies and luminosities (we only include the PP set giving the lowest error)

| $\sqrt{s} = 0.5 \text{ TeV}$ | | | | | | $\sqrt{s} = 1 \text{ TeV}$ | | | | | |
|---------------------------------------|--------------------|----|----------------------|----------------------|-----------------------|---------------------------------------|--------------------|----|----------------------|----------------------|-----------------------|
| $\overline{\Delta c_i}$ | ϕ | PP | 100 fb ⁻¹ | 500 fb ⁻¹ | 1000 fb ⁻¹ | $\overline{\Delta c_i}$ | ϕ | PP | 100 fb ⁻¹ | 500 fb ⁻¹ | 1000 fb ⁻¹ |
| $\overline{\Delta \mathcal{F}_L}$ | $\cos \theta_{te}$ | 8 | 0.10 | 0.046 | 0.033 | $\overline{\Delta \mathcal{F}_L}$ | $\cos \theta_{te}$ | 4 | 0.036 | 0.016 | 0.011 |
| $\overline{\Delta \mathcal{F}_R}$ | $\cos \theta_{te}$ | 3 | 0.12 | 0.054 | 0.038 | $\overline{\Delta \mathcal{F}_R}$ | p_T^b | 1 | 0.026 | 0.012 | 0.0083 |
| $\overline{\Delta \mathcal{G}'_{4f}}$ | E_T | 6 | 0.13 | 0.059 | 0.042 | $\overline{\Delta \mathcal{G}'_{4f}}$ | p_T^b | 4 | 0.049 | 0.022 | 0.016 |

where $f_i(\phi)$ are known functions and c_i are model-dependent coefficients; the goal is to determine the accuracy to which the c_i can be measured.

Denoting the statistical uncertainty in c_i by Δc_i , the optimized covariance matrix equals

$$V_{ij} = \langle \Delta c_i \Delta c_j \rangle = \frac{\sigma_T}{N} X_{ij}, \quad (13)$$

where $\sigma_T = \int \Sigma(\phi) d\phi$, N is the total number of events and X_{ij} is obtained from

$$(X^{-1})_{ij} = \int \frac{f_i(\phi) f_j(\phi)}{\Sigma(\phi)} d\phi. \quad (14)$$

In particular, the minimum uncertainty in the measurement of c_i is given by

$$\overline{\Delta c_i} = \sqrt{\langle (\Delta c_i)^2 \rangle} = \sqrt{\frac{\sigma_T}{N} X_{ii}} \quad (15)$$

To order of $1/\Lambda^2$ we can write

$$\frac{d\sigma}{d\phi} = f_{SM}(\phi) + \mathcal{F}_L f_{\mathcal{F}_L}(\phi) + \mathcal{F}_R f_{\mathcal{F}_R}(\phi) + \mathcal{G}'_{4f} f_{\mathcal{G}'_{4f}}(\phi). \quad (16)$$

where \mathcal{G}'_{4f} is defined in (10). To this order we need only calculate $(X^{-1})_{ij}$ with $i, j = 1, 2, 3, 4$ corresponding to SM, \mathcal{F}_L , \mathcal{F}_R and \mathcal{G}_{4f} , respectively, and then obtain $\overline{\Delta c_i}$ using (15) taking $\sigma_T = \int d\phi f_{SM}(\phi)$.

In Table IV we present the choice of PP and kinematic variable that minimize the statistical uncertainty for the effective operator parameters. We note that the best choice for \mathcal{F}_R corresponds to PP sets (1) or (3) that enlarge the right-handed polarized photon beam.

These result indicate the possibility of measuring these couplings at the 5% accuracy (at the 1σ level) in a $\sqrt{s} = 0.5 \text{ TeV}$ collider with a luminosity of 500 fb^{-1} . If we denote by Λ_{\max}

the largest scale that can be probed with a given measurement then, using the expressions for $\mathcal{F}_L, \mathcal{F}_R$ (Eq. 5) with $C_i \sim 1$, this corresponds to a reach up to $\Lambda_{\max} = 1$ TeV; using \mathcal{G}_{4f} this becomes $\Lambda_{\max} = 5$ TeV. For $\sqrt{s} = 1$ TeV and a luminosity of 1000 fb^{-1} the corresponding values are $\Lambda_{\max} = 1$ TeV and 10 TeV respectively.

The types of physics being probed are quite different: a bound on $\mathcal{F}_L, \mathcal{F}_R$ constrains a combination of the mixing angles of the t and b with heavy generations and those of the W with a heavy W' and the masses of these heavy excitations; a bound on \mathcal{G}_{4f} constrains a combination of fermion couplings to heavy W' and/or leptoquarks and the masses of these particles.

B. Distinguishing models

As mentioned above the effective operators contributing to the reaction $e\gamma \rightarrow tb\nu$ can be generated by a variety of heavy particles. Below we consider several models:

- Normal W' model:

An extra gauge boson W' arises in many extension of the SM [36, 37, 38, 39, 40, 41, 42, 43, 44, 45, 46, 47]. Here we only consider the simplest case where the new gauge boson (W') has the same couplings as the SM W boson. If we also assume no $W - W'$ mixing the low-energy W' effects correspond to

$$\mathcal{F}_L = 0, \quad \mathcal{G}'_{4f} = -\frac{g^2}{2} \left(\frac{1 \text{ TeV}}{\Lambda} \right)^2, \quad \Lambda = m_{W'}. \quad (17)$$

When $m_{W'} = 1$ TeV, $\mathcal{G}_{4f} = 0.21$.

- Hexagonal $SU(3)$ unification model [48]

In this supersymmetric model the original $SU(3)^6$ symmetry is broken to $SU(2)_A \times SU(2)_B$ at a high scale which break to $SU(2)$ at the SUSY braking scale. As a result a second set of weak gauge bosons appear at this stage, with the coupling of the W' boson to the SM particles is completely fixed by the underlying of theory; the salient feature of this model is that the W' boson couples to the leptons and quarks differently. In general, the SM W boson can mix with W' boson but for illustration, we consider the simplest case where there is no $W - W'$ mixing; then

$$\mathcal{F}_L = 0, \quad \mathcal{G}'_{4f} = -\frac{g^2}{2} \frac{g_A}{g_B} \left(\frac{g_A}{g_B} \cos^2 \theta - \frac{g_B}{g_A} \sin^2 \theta \right) \left(\frac{1 \text{ TeV}}{\Lambda} \right)^2, \quad \Lambda = m_{W'}. \quad (18)$$

where $g_A = 0.71$, $g_B = 1.63$ are the $SU(2)_{A,B}$ gauge couplings (fixed by the unification condition), and θ is the mixing angle that determines the coupling of the W' to the leptons (it depends only on $M_{W'}/M_W$). When $m_{W'}^2 = 1 \text{ TeV}$, $\theta \simeq 0.4$ and $\mathcal{G}'_{4f} = 0.05$.

- Little Higgs Model with T-parity [49, 50, 51]

The LH model can be extended to include a discrete symmetry, T-parity, which greatly reduces the new-physics contributions to precision electroweak observables [51]. In particular, light and heavy gauge bosons have opposite charges under T-parity and do not mix; the four-fermion operator in Eq. 7 is not generated (at tree level) for the same reason. Nonetheless the Wtb is modified by the mixing of the top quark with its T-even partner is still present and shifts the coupling sizably through the mixing with the SM top quark. In our notation,

$$\mathcal{F}_L = -\frac{c_\lambda^4 v^2}{2 f^2}, \quad \mathcal{F}_R = 0, \quad \mathcal{G}'_{4f} = 0, \quad \Lambda = 4\pi f \quad (19)$$

where $c_\lambda = \lambda_1/\sqrt{\lambda_1^2 + \lambda_2^2}$. Here $\lambda_{1,2}$ denote the Yukawa couplings giving masses to the top quark and its heavy partners, and $4\pi f$ the heavy symmetry breaking scale. In this study, we choose $c_\lambda = 1/\sqrt{2}$, $\mathcal{F}_L = 0.015$ (0.007) for $f = 0.7$ (1) TeV.

The 2σ bounds of the anomalous couplings parameter space, within which no distinction from the SM is possible, are shown in Fig. 7. In the figure we also show the theory predictions of the three models described above. It is clear that the single top production process in the $e\gamma$ collision can be used to distinguish various models which include either \mathcal{F}_L or \mathcal{G}'_{4f} effect coupling (the \mathcal{F}_R coupling is not included since the error of its measurement is much larger than its value).

V. CONCLUSIONS

In this paper we have considered single-top production in $e\gamma$ colliders as a probe for new physics effects, assuming that the collider energy is not sufficiently high to directly probe these effects. We argued that for natural theories the deviations from the SM tree-level couplings in this reaction can be parameterized by 3 couplings; one of these (\mathcal{F}_R) is very strongly constrained by the data while another (\mathcal{F}_L) affects only the overall cross-section normalization.

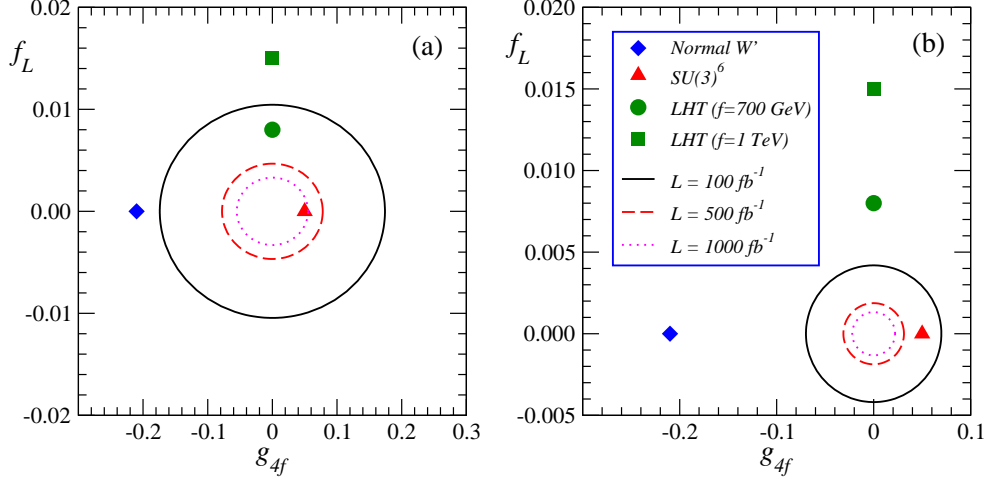


FIG. 7: 2σ contours of the total cross section within the models studied in the text (a) $\sqrt{s} = 500$ GeV, (b) $\sqrt{s} = 1$ TeV (assuming $m_{W'} = f = 1$ TeV and $\mathcal{F}_R = 0$).

Of the observables studied the missing energy, transverse top-quark momentum and scattering angle proved best for distinguishing the effects of the various effective couplings. An optimal observable analysis (table IV) shows that these coefficients can be measured with $3\text{-}\sigma$ accuracy down to the 10-5% level depending on the collider energy and luminosity; for a luminosity of 1000 fb^{-1} this allows to probe physics at scales up to 1.5 times the collider center mass energy. Even the use of a broad observable such as the total cross section can be used to probe new physics effects at similar levels.

These results, however, will be diluted when realistic detector effects are included in the analysis. It is also noteworthy that the deviations from the SM do not show up as unexpected peaks but as an excess or deficiency of events in various kinematic regions which can be reliably determined only if the details of the detectors are well understood and sufficiently large number of events has been accrued. Still we believe that the above features are of sufficient interest to warrant further study of this reaction.

Acknowledgments

Q.-H. Cao thanks C.-P. Yuan for many useful discussions. Q.-H. Cao and J. Wudka are supported in part by the U.S. Department of Energy under grant No. DE-FG03-94ER40837.

APPENDIX A: PHOTON DISTRIBUTION FUNCTIONS

The photon distribution functions have been given with details in [52]. For the sake of completeness, we also list them here.

At a linear collider the single top quarks can be produced from the following two processes:

$$t : e^+ \gamma \rightarrow \bar{\nu} t \bar{b}, \quad \bar{t} : e^- \gamma \rightarrow \nu b \bar{t}, \quad (\text{A1})$$

where the photon comes from the original incoming electron and positron, respectively. The total cross sections for these two processes at a linear collider are

$$\begin{aligned} \sigma(e^- e^+ \rightarrow \bar{\nu} t \bar{b}) &= \int dx \frac{dN(x)}{dx} \hat{\sigma}(e^+ \gamma \rightarrow \bar{\nu} t \bar{b}), \\ \sigma(e^- e^+ \rightarrow \nu b \bar{t}) &= \int dy \frac{dN(y)}{dy} \hat{\sigma}(e^- \gamma \rightarrow \nu b \bar{t}), \end{aligned} \quad (\text{A2})$$

where dN/dy is the photon-spectral function (equivalent to the parton distribution function inside hadrons). Here x (y) denotes the fraction of the electron (positron) momentum carried by the photons: $p_\gamma = xp_{e^-}$ and $p_\gamma = yp_{e^+}$.

Using the spin density matrix method to keep track on the photon polarization, the hard cross section the processes (A1) take the form

$$\hat{\sigma}(e^+ \gamma \rightarrow \bar{\nu} t \bar{b}) = \frac{1}{2} N_c \sum_{a,b=\pm} \frac{1}{2\hat{s}} \int d\Pi_3 \rho^{ab}(x) \mathcal{M}_a(e^+ \gamma \rightarrow \bar{\nu} t \bar{b}) \mathcal{M}_b^*(e^+ \gamma \rightarrow \bar{\nu} t \bar{b}), \quad (\text{A3})$$

$$\hat{\sigma}(e^- \gamma \rightarrow \nu b \bar{t}) = \frac{1}{2} N_c \sum_{a,b=\pm} \frac{1}{2\hat{s}} \int d\Pi_3 \rho^{ab}(y) \mathcal{M}_a(e^- \gamma \rightarrow \nu b \bar{t}) \mathcal{M}_b^*(e^- \gamma \rightarrow \nu b \bar{t}), \quad (\text{A4})$$

where the factor of $1/2$ comes from averaging over the initial-state electron or positron spin (it should be replaced by 1 for the purely polarized electron or positron beam), $N_c = 3$ is the color factor by summing over the color of the final state quarks, $d\Pi_3$ represents 3-body final-state phase space, and ρ^{ab} is the photon polarization density matrices; the helicity amplitudes \mathcal{M} are given in the next section. Here, \hat{s} is the square of the sub-process beam energy: $\hat{s} = (p_{e^+} + p_\gamma)^2$ for $e^+ \gamma$ collision or $\hat{s} = (p_{e^-} + p_\gamma)^2$ for $e^- \gamma$ collision. The spin-averaging factor for the incoming photon has been included in the spin density matrices ρ^{ab} .

The density matrix ρ is not only a function of the momentum fraction x or y , but also depends on the choice of the photon polarization vectors. In $e^+ - \gamma$ collisions we take the

positron moving along the $-\hat{z}$ direction and the photon scattered from the incoming electron along the $+\hat{z}$ direction, therefore, its polarization vectors are defined as:

$$\epsilon^\mu(h_1) = \frac{1}{\sqrt{2}}(\epsilon_1^\mu + ih_1\epsilon_2^\mu), \quad (\text{A5})$$

where h_1 is the helicity of the photon with $\epsilon_1^\mu = (0, 1, 0, 0)$ and $\epsilon_2^\mu = (0, 0, 1, 0)$.

In $e^-\gamma$ collisions we take the electron moving along the $+\hat{z}$ direction; the photon is scattered off the incoming positron and moves along $-\hat{z}$ direction, therefore its polarization vectors are defined as

$$\epsilon^\mu(h_2) = \frac{1}{\sqrt{2}}(-\epsilon_1^\mu + ih_2\epsilon_2^\mu), \quad (\text{A6})$$

where h_2 is the helicity of the photon.

With these choices the density matrices $\rho(x)$ and $\rho(y)$ in terms of the three Stokes parameters ξ_i are given by

$$\rho(x) = \frac{1}{2} \begin{pmatrix} 1 + \xi_2(x) & \xi_3(x) - i\xi_1(x) \\ \xi_3(x) + i\xi_1(x) & 1 - \xi_2(x) \end{pmatrix}, \quad (\text{A7})$$

$$\rho(y) = \frac{1}{2} \begin{pmatrix} 1 - \xi_2(y) & \xi_3(y) + i\xi_1(y) \\ \xi_3(y) - i\xi_1(y) & 1 + \xi_2(y) \end{pmatrix}. \quad (\text{A8})$$

The maximum of x and y is given by

$$x_{max} = \frac{x_0}{1 + x_0}, \quad y_{max} = \frac{y_0}{1 + y_0}. \quad (\text{A9})$$

Here x_0 (y_0) determines the upper limit of the final photon energy,

$$E_\gamma^{max} = \frac{x_0}{1 + x_0} E_e. \quad (\text{A10})$$

The larger the value for x_0 is chosen the more energy can be transferred to the photon. However, to suppress pair production we must require

$$x_0(y_0) \leq 2 \left(1 + \sqrt{2}\right) \sim 4.828. \quad (\text{A11})$$

The photon-spectrum function $dN(x)/dx$ and $\xi_i(x)$ in the spin density matrix $\rho(x)$ immediately after its production at the conversion point are given by the following formulas:

$$\frac{dN(x)}{dx} = \frac{C(x)}{D(x_0)},$$

$$\begin{aligned}
\xi_1(x) &= \frac{2\mathcal{P}_t \sin(2\varphi) [r(x)^2]}{C(y)}, \\
\xi_2(x) &= \frac{\mathcal{P}_e f_2(x) + \mathcal{P}_\gamma f_3(x)}{C(y)}, \\
\xi_3(x) &= \frac{2\mathcal{P}_t \cos(2\varphi) [r(x)^2]}{C(x)},
\end{aligned} \tag{A12}$$

where

$$\begin{aligned}
C(x) &= f_0(y) + \mathcal{P}_e \mathcal{P}_\gamma f_1(x), \\
D(x_0) &= D_0(x_0) + \mathcal{P}_e \mathcal{P}_\gamma D_1(x_0), \\
f_0(x) &= \frac{1}{1-y} + 1 - x - 4r(x) [1 - r(x)], \\
f_1(x) &= \frac{y(2-x) [1 - 2r(x)]}{1-y}, \\
f_2(x) &= y_0 r(x) \{1 + (1-x) [1 - 2r(x)]^2\}, \\
f_3(x) &= [1 - 2r(x)] \left[\frac{1}{1-x} + 1 - x \right], \\
r(x) &= \frac{x}{x_0(1-x)}, \\
D_0(x_0) &= \left(1 - \frac{4}{x_0} - \frac{8}{x_0^2} \right) \ln(1+x_0) + \frac{1}{2} + \frac{8}{x_0} - \frac{1}{2(1+x_0)^2}, \\
D_1(x_0) &= \left(1 + \frac{2}{x_0} \right) \ln(1+x_0) - \frac{5}{2} + \frac{1}{1+x_0} - \frac{1}{2(1+x_0)^2},
\end{aligned} \tag{A13}$$

$dN(y)/dy$ and $\xi_i(y)$ are obtained by replacing \mathcal{P}_e , \mathcal{P}_γ and \mathcal{P}_t by $\mathcal{P}_{\bar{e}}$, $\mathcal{P}_{\bar{\gamma}}$ and $\mathcal{P}_{\bar{t}}$. Here \mathcal{P}_e and $\mathcal{P}_{\bar{e}}$ is the longitudinal-polarization of the incoming electron (positron), respectively, with the definition as

$$\mathcal{P}_e = \frac{N_+ - N_-}{N_+ + N_-}, \quad \mathcal{P}_{\bar{e}} = -\frac{N_+ - N_-}{N_+ + N_-}, \tag{A14}$$

where N_\pm respectively denote the number of electrons or positrons with positive and negative helicities. \mathcal{P}_γ and $\mathcal{P}_{\bar{\gamma}}$ represent the average helicities of the initial-laser-photons, and \mathcal{P}_t and $\mathcal{P}_{\bar{t}}$ represents the maximum average linear-polarization of the initial-laser-photons. The azimuthal angle φ is defined in the same way as in [13]. We note that $\mathcal{P}_{\gamma,t}$ and $\mathcal{P}_{\bar{\gamma},\bar{t}}$ obey

$$0 \leq \mathcal{P}_\gamma^2 + \mathcal{P}_t^2 \leq 1, \quad 0 \leq \mathcal{P}_{\bar{\gamma}}^2 + \mathcal{P}_{\bar{t}}^2 \leq 1. \tag{A15}$$

In Fig. 8 we show the effective photon spectrum distributions as a function of x with the polarization parameter sets listed in Table I. It is clearly shown that colliding like-handed electrons and photons results in a flat distribution of backscattered photons while colliding oppositely handed electrons and photons results in a peaked distribution of backscattered photons. In both cases the resulting photons are highly polarized [13].

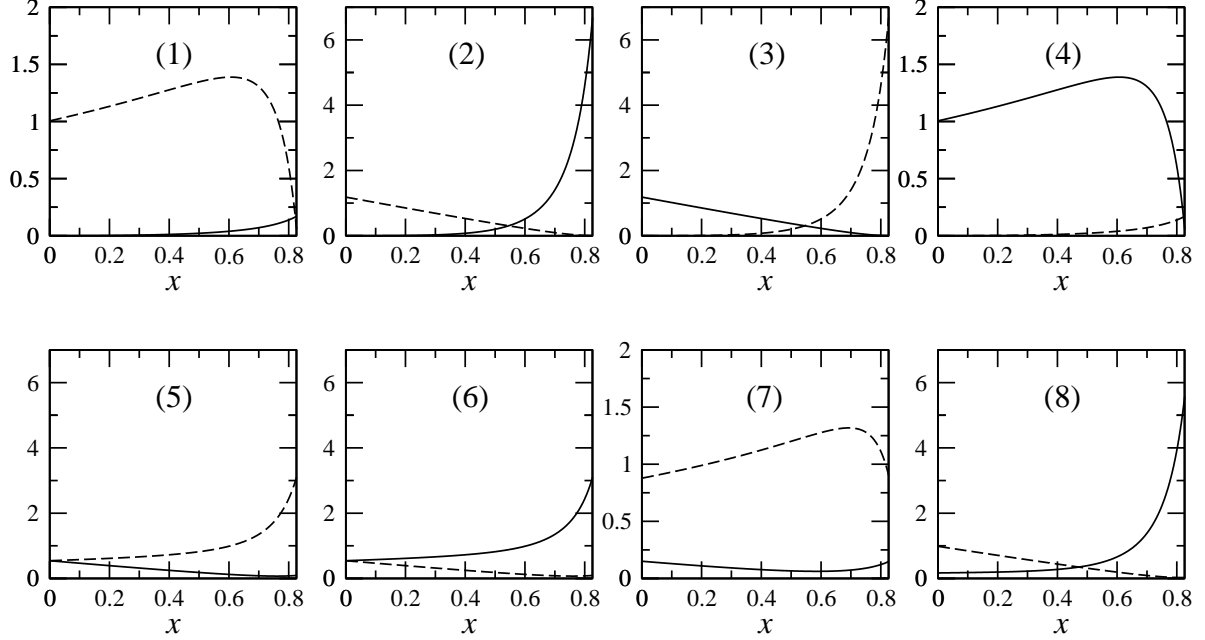


FIG. 8: The photon spectrum distributions as a function of x for various choices of the polarization parameters listed in Table. I. The solid curve in each plot denotes the spectrum of negative helicity photons ($\rho(2,2)$) while the dashed curve denotes that of positive helicity photons $\rho(1,1)$.

APPENDIX B: HELICITY AMPLITUDES

1. Notation

In this appendix we briefly summarize our method for calculating the helicity amplitudes. The method breaks down the algebra of four-dimensional Dirac spinors and matrices into equivalent two-dimensional ones. In the Weyl basis, Dirac spinors have the form

$$\begin{pmatrix} \psi_+ \\ \psi_- \end{pmatrix}, \quad (\text{B1})$$

where for fermions

$$\psi_{\pm} = \begin{cases} u_{\pm}^{(\lambda=+)} = \omega_{\pm} \chi_{1/2} & , \\ u_{\pm}^{(\lambda=-)} = \omega_{\mp} \chi_{-1/2} & , \end{cases} \quad (\text{B2})$$

and anti-fermions

$$\psi_{\pm} = \begin{cases} v_{\pm}^{(\lambda=1)} = \pm \omega_{\mp} \chi_{-1/2} & , \\ v_{\pm}^{(\lambda=-)} = \mp \omega_{\pm} \chi_{1/2} & , \end{cases} \quad (\text{B3})$$

with $\omega_\lambda = \sqrt{E + \lambda|\vec{p}|}$; $\lambda = \pm 1$, where E and \vec{p} are the energy and momentum of the fermion, respectively. The $\chi_{\lambda/2}$'s are eigenvectors of the helicity operator

$$h = \hat{p} \cdot \sigma, \text{ with } \hat{p} = \vec{p}/|\vec{p}|, \quad (\text{B4})$$

where eigenvalue $\lambda = 1$ is for “spin-up” and $\lambda = -1$ is for “spin-down” fermion.

$$\chi_{1/2} \equiv |\hat{p}+\rangle = \begin{pmatrix} \cos \theta/2 \\ e^{i\phi} \sin \theta/2 \end{pmatrix}, \quad \chi_{-1/2} \equiv |\hat{p}-\rangle = \begin{pmatrix} -e^{i\phi} \sin \theta/2 \\ \cos \theta/2 \end{pmatrix}, \quad (\text{B5})$$

where we introduce the shorthand notations $|\hat{p}, \pm\rangle$ for $\chi_{\pm 1/2}$. We can further simplify (B2, B3) using the notation

$$u_\pm(\lambda) = \omega_{\pm\lambda} |\hat{p}, \lambda\rangle, \quad v_\pm(\lambda) = \pm\lambda\omega_{\mp\lambda} |\hat{p}, -\lambda\rangle, \quad (\text{B6})$$

Gamma matrices in the Weyl basis have the form

$$\gamma^0 = \begin{pmatrix} 0 & 1 \\ 1 & 0 \end{pmatrix}, \quad \gamma^j = \begin{pmatrix} 0 & -\sigma_j \\ \sigma_j & 0 \end{pmatrix}, \quad \gamma^5 = \begin{pmatrix} 1 & 0 \\ 0 & -1 \end{pmatrix}, \quad (\text{B7})$$

where σ_j are the Pauli 2×2 spin matrices. In the Weyl basis, \not{p} takes the form

$$\not{p} \equiv p_\mu \gamma^\mu = \begin{pmatrix} 0 & p_0 + \vec{\sigma} \cdot \vec{p} \\ p_0 - \vec{\sigma} \cdot \vec{p} & 0 \end{pmatrix} \equiv \begin{pmatrix} 0 & \not{p}_+ \\ \not{p}_- & 0 \end{pmatrix} \equiv p_\mu \begin{pmatrix} 0 & \gamma_+^\mu \\ \gamma_-^\mu & 0 \end{pmatrix} \quad (\text{B8})$$

where

$$\gamma_\pm^\mu = (1, \mp \vec{\sigma}). \quad (\text{B9})$$

2. Wtb operators

For the process $e^- \gamma \rightarrow \nu b \bar{t}$, the Feynman diagram involving the effective $W - t - b$ couplings are shown in Fig. 9. Unitary gauge is adopted in our calculation. We denote the helicity amplitude as $\mathcal{M}_{Wtb}(\lambda_\gamma, \lambda_b, \lambda_{\bar{t}})$ where λ_γ , λ_b and $\lambda_{\bar{t}}$ is the helicity of γ , b and \bar{t} , respectively. Below we give the the helicity amplitudes of process $e^- \gamma \rightarrow \nu b \bar{t}$ which are induced by the effective Wtb coupling defined in (4):

$$\mathcal{M}_{Wtb}(\lambda_\gamma, \lambda_b, \lambda_{\bar{t}}) = \left(i \frac{g}{\sqrt{2}} \right)^2 (ie) (\omega_+^e \omega_+^\nu)$$

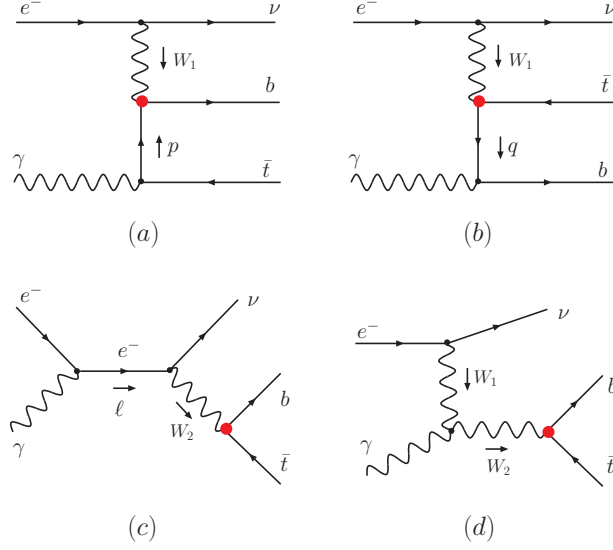


FIG. 9: Feynman diagrams of process $e^- \gamma \rightarrow \nu b \bar{t}$ which involve effective $W - t - b$ couplings (\mathcal{F}_L and \mathcal{F}_R) denoted by the red circle. The arrow lines beside the propagators indicate the momentum assignments used in the helicity amplitude calculation.

$$\begin{aligned}
& \times \left\{ \frac{Q_{\bar{t}}}{(p_{W_1}^2 - m_W^2 + im_W \Gamma_W)(p^2 - m_t^2)} \mathcal{M}_{Wtb}^a(\lambda_\gamma, \lambda_b, \lambda_{\bar{t}}) \right. \\
& + \frac{Q_b}{(p_{W_1}^2 - m_W^2 + im_W \Gamma_W)(q^2 - m_b^2)} \mathcal{M}_{Wtb}^b(\lambda_\gamma, \lambda_b, \lambda_{\bar{t}}) \\
& + \frac{1}{(p_{W_2}^2 - m_W^2 + im_W \Gamma_W) \ell^2} \mathcal{M}_{Wtb}^c(\lambda_\gamma, \lambda_b, \lambda_{\bar{t}}) \\
& \left. + \frac{1}{(p_{W_1}^2 - m_W^2 + im_W \Gamma_W)(p_{W_2}^2 - m_W^2 + im_W \Gamma_W)} \mathcal{M}_{Wtb}^d(\lambda_\gamma, \lambda_b, \lambda_{\bar{t}}) \right\} \quad (\text{B10})
\end{aligned}$$

where

$$\begin{aligned}
\mathcal{M}_{Wtb}^a(\lambda_\gamma, \lambda_b, \lambda_{\bar{t}}) &= 2\mathcal{F}_L [\omega_{-\lambda_b} (-\lambda_{\bar{t}} \omega_{\lambda_{\bar{t}}})] \langle e, + | \not{p}_- \not{\epsilon}_+ | \bar{t}, -\lambda_{\bar{t}} \rangle \langle b, \lambda_b | \nu, + \rangle \\
&+ 2\mathcal{F}_R [\omega_{\lambda_b} (\lambda_{\bar{t}} \omega_{-\lambda_{\bar{t}}})] \langle \nu, - | \not{p}_+ \not{\epsilon}_- | \bar{t}, -\lambda_{\bar{t}} \rangle \langle b, \lambda_b | e, - \rangle \\
&+ 2\mathcal{F}_L m_t [\omega_{-\lambda_b} (\lambda_{\bar{t}} \omega_{-\lambda_{\bar{t}}})] \langle e, + | \not{\epsilon}_- | \bar{t}, -\lambda_{\bar{t}} \rangle \langle b, \lambda_b | \nu, + \rangle \\
&+ 2\mathcal{F}_R m_t [\omega_{\lambda_b} (-\lambda_{\bar{t}} \omega_{\lambda_{\bar{t}}})] \langle \nu, - | \not{\epsilon}_+ | \bar{t}, -\lambda_{\bar{t}} \rangle \langle b, \lambda_b | e, - \rangle, \quad (\text{B11})
\end{aligned}$$

$$\begin{aligned}
\mathcal{M}_{Wtb}^b(\lambda_\gamma, \lambda_b, \lambda_{\bar{t}}) &= 2\mathcal{F}_L [\omega_{-\lambda_b} (-\lambda_{\bar{t}} \omega_{\lambda_{\bar{t}}})] \langle b, \lambda_b | \not{\epsilon}_+ \not{q}_- | \nu, + \rangle \langle e, + | \bar{t}, -\lambda_{\bar{t}} \rangle \\
&+ 2\mathcal{F}_R [\omega_{\lambda_b} (\lambda_{\bar{t}} \omega_{-\lambda_{\bar{t}}})] \langle b, \lambda_b | \not{\epsilon}_- \not{q}_+ | e, - \rangle \langle \nu, - | \bar{t}, -\lambda_{\bar{t}} \rangle
\end{aligned}$$

$$\begin{aligned}
& + 2\mathcal{F}_L m_b [\omega_{\lambda_b} (-\lambda_{\bar{t}} \omega_{\lambda_{\bar{t}}})] \langle b, \lambda_b | \not{\epsilon}_- | \nu, + \rangle \langle e, + | \bar{t}, -\lambda_{\bar{t}} \rangle \\
& + 2\mathcal{F}_R m_b [\omega_{-\lambda_b} (\lambda_{\bar{t}} \omega_{-\lambda_{\bar{t}}})] \langle b, \lambda | \not{\epsilon}_+ | e, - \rangle \langle \nu, - | \bar{t}, -\lambda_{\bar{t}} \rangle, \tag{B12}
\end{aligned}$$

$$\begin{aligned}
\mathcal{M}_{Wtb}^c(\lambda_\gamma, \lambda_b, \lambda_{\bar{t}}) & = 2\mathcal{F}_L [\omega_{-\lambda_b} (-\lambda_{\bar{t}} \omega_{\lambda_{\bar{t}}})] \langle b, \lambda_b | \nu, + \rangle \langle e, + | \not{\epsilon}_- \not{\epsilon}_+ | \bar{t}, -\lambda_{\bar{t}} \rangle \\
& + 2\mathcal{F}_R [\omega_{\lambda_b} (\lambda_{\bar{t}} \omega_{-\lambda_{\bar{t}}})] \langle \nu, - | \bar{t}, -\lambda_{\bar{t}} \rangle \langle b, \lambda_b | \not{\epsilon}_- \not{\epsilon}_+ | e, - \rangle \\
& - \frac{\mathcal{F}_L}{m_W^2} \left[m_b \omega_{\lambda_b} (-\lambda_{\bar{t}} \omega_{\lambda_{\bar{t}}}) - m_t \omega_{-\lambda_b} (\lambda_{\bar{t}} \omega_{-\lambda_{\bar{t}}}) \right] \\
& \quad \times \langle b, \lambda_b | \bar{t}, -\lambda_{\bar{t}} \rangle \langle \nu, - | \not{p}_{W_2+} \not{\epsilon}_- \not{\epsilon}_+ | e, - \rangle \\
& - \frac{\mathcal{F}_R}{m_W^2} \left[m_b \omega_{-\lambda_b} (\lambda_{\bar{t}} \omega_{-\lambda_{\bar{t}}}) - m_t \omega_{\lambda_b} (-\lambda_{\bar{t}} \omega_{\lambda_{\bar{t}}}) \right] \\
& \quad \times \langle b, \lambda_b | \bar{t}, -\lambda_{\bar{t}} \rangle \langle \nu, - | \not{p}_{W_2+} \not{\epsilon}_- \not{\epsilon}_+ | e, - \rangle, \tag{B13}
\end{aligned}$$

$$\begin{aligned}
\mathcal{M}_{Wtb}^d(\lambda_\gamma, \lambda_b, \lambda_{\bar{t}}) & = -\mathcal{F}_L [\omega_{-\lambda_b} (-\lambda_{\bar{t}} \omega_{\lambda_{\bar{t}}})] \\
& \quad \times \left[2 \langle b, \lambda_b | \nu, + \rangle \langle e, + | \bar{t}, -\lambda_{\bar{t}} \rangle (p_{W_1} + p_{W_2}) \cdot \epsilon \right. \\
& \quad \left. - \langle \nu, - | (\not{p}_{W_2+} \not{p}_\gamma)_+ | e, - \rangle \langle b, \lambda_b | \not{\epsilon}_+ | \bar{t}, -\lambda_{\bar{t}} \rangle \right. \\
& \quad \left. + \langle \nu, - | \not{\epsilon}_+ | e, - \rangle \langle b, \lambda_b | (\not{p}_\gamma - \not{p}_{W_1})_+ | \bar{t}, -\lambda_{\bar{t}} \rangle \right] \\
& - \mathcal{F}_R [\omega_{\lambda_b} (\lambda_{\bar{t}} \omega_{-\lambda_{\bar{t}}})] \\
& \quad \times \left[2 \langle \nu, - | \bar{t}, -\lambda_{\bar{t}} \rangle \langle b, \lambda_b | e, - \rangle (p_{W_1} + p_{W_2}) \cdot \epsilon \right. \\
& \quad \left. - \langle \nu, - | (\not{p}_{W_2+} \not{p}_\gamma)_+ | e, - \rangle \langle b, \lambda_b | \not{\epsilon}_- | \bar{t}, -\lambda_{\bar{t}} \rangle \right. \\
& \quad \left. + \langle \nu, - | \not{\epsilon}_+ | e, - \rangle \langle b, \lambda_b | (\not{p}_\gamma - \not{p}_{W_1})_- | \bar{t}, -\lambda_{\bar{t}} \rangle \right] \\
& + \mathcal{F}_L \frac{2p_e \cdot p_\gamma}{m_W^2} \left[m_b \omega_{\lambda_b} (-\lambda_{\bar{t}} \omega_{\lambda_{\bar{t}}}) - m_t \omega_{-\lambda_b} (\lambda_{\bar{t}} \omega_{-\lambda_{\bar{t}}}) \right] \\
& \quad \times \langle b, \lambda_b | \bar{t}, -\lambda_{\bar{t}} \rangle \langle \nu, - | \not{\epsilon}_+ | e, - \rangle \\
& + \mathcal{F}_R \frac{2p_e \cdot p_\gamma}{m_W^2} \left[m_b \omega_{-\lambda_b} (\lambda_{\bar{t}} \omega_{-\lambda_{\bar{t}}}) - m_t \omega_{\lambda_b} (-\lambda_{\bar{t}} \omega_{\lambda_{\bar{t}}}) \right] \\
& \quad \times \langle b, \lambda_b | \bar{t}, -\lambda_{\bar{t}} \rangle \langle \nu, - | \not{\epsilon}_+ | e, - \rangle, \tag{B14}
\end{aligned}$$

where $\lambda_\gamma, \lambda_b, \lambda_{\bar{t}} = \mp 1$ corresponds to left-handed and right-handed helicity respectively. The momentum of the propagators are defined as follows: $p_{W_1} = p_e - p_\nu$, $p_{W_2} = p_b + p_{\bar{t}}$, $p = p_\gamma - p_b$, $q = p_\gamma - p_{\bar{t}}$, $\ell = p_\gamma + p_{e^-}$, cf. Fig. 9, and $\epsilon(\lambda_\gamma)$ is the polarization vector of the incoming photon. The weight factor ω_{λ_i} depends on the helicity (λ_i) of the fermion i :

$$\omega_{\lambda_i} \equiv \sqrt{E_i + \lambda_i |\vec{p}_i|}, \tag{B15}$$

where E_i and \vec{p}_i is the energy and momentum of the fermion i , respectively.

It is very straightforward to get the SM helicity amplitudes from by setting $\mathcal{F}_L = 1$, and $\mathcal{F}_R = 0$.

3. Four-fermion operator

The Feynman diagrams involving effective 4-fermion couplings are shown in Fig. 10. Denoting the helicity amplitude as $\mathcal{M}_{4f}(\lambda_\gamma, \lambda_b, \lambda_{\bar{t}})$ where λ_γ , λ_b and $\lambda_{\bar{t}}$ is the helicity of γ , b and \bar{t} , respectively, we obtain the matrix element as follows:

$$\begin{aligned} \mathcal{M}_{4f}(\lambda_\gamma, \lambda_b, \lambda_{\bar{t}}) &= (i\mathcal{G}_{4f})(ie)(\omega_+^e \omega_+^\nu) \\ &\times \left\{ \frac{Q_{\bar{t}}}{p^2 - m_{\bar{t}}^2} \mathcal{M}_{4f}^a(\lambda_\gamma, \lambda_b, \lambda_{\bar{t}}) + \frac{Q_b}{q^2 - m_b^2} \mathcal{M}_{4f}^b(\lambda_\gamma, \lambda_b, \lambda_{\bar{t}}) \right. \\ &\left. + \frac{1}{\ell^2} \mathcal{M}_{4f}^c(\lambda_\gamma, \lambda_b, \lambda_{\bar{t}}) \right\}, \end{aligned} \quad (\text{B16})$$

where

$$\begin{aligned} \mathcal{M}_{4f}^a(\lambda_\gamma, \lambda_b, \lambda_{\bar{t}}) &= 2[\omega_{-\lambda_b}(-\lambda_{\bar{t}}\omega_{\lambda_{\bar{t}}})] \langle e, + | \not{p}_- \not{\epsilon}_+ | \bar{t}, -\lambda_{\bar{t}} \rangle \langle b, \lambda_b | \nu, + \rangle \\ &+ 2m_t[\omega_{-\lambda_b}(\lambda_{\bar{t}}\omega_{-\lambda_{\bar{t}}})] \langle e, + | \not{\epsilon}_- | \bar{t}, -\lambda_{\bar{t}} \rangle \langle b, \lambda_b | \nu, + \rangle, \end{aligned} \quad (\text{B17})$$

$$\begin{aligned} \mathcal{M}_{4f}^b(\lambda_\gamma, \lambda_b, \lambda_{\bar{t}}) &= 2[\omega_{-\lambda_b}(-\lambda_{\bar{t}}\omega_{\lambda_{\bar{t}}})] \langle b, \lambda_b | \not{\epsilon}_+ \not{q}_- | \nu, + \rangle \langle e, + | \bar{t}, -\lambda_{\bar{t}} \rangle \\ &+ 2m_b[\omega_{\lambda_b}(-\lambda_{\bar{t}}\omega_{\lambda_{\bar{t}}})] \langle b, \lambda_b | \not{\epsilon}_- | \nu, + \rangle \langle e, + | \bar{t}, -\lambda_{\bar{t}} \rangle, \end{aligned} \quad (\text{B18})$$

$$\mathcal{M}_{4f}^c(\lambda_\gamma, \lambda_b, \lambda_{\bar{t}}) = 2[\omega_{-\lambda_b}(-\lambda_{\bar{t}}\omega_{\lambda_{\bar{t}}})] \langle b, \lambda_b | \nu, + \rangle \langle e, + | \not{\epsilon}_- \not{\epsilon}_+ | \bar{t}, -\lambda_{\bar{t}} \rangle, \quad (\text{B19})$$

where the momentum of propagators is the same as the ones of effective Wtb couplings.

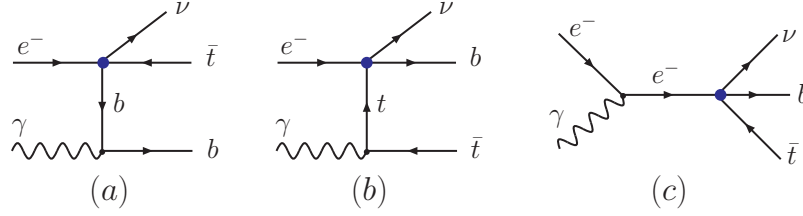


FIG. 10: Feynman diagrams of process $e^- \gamma \rightarrow \nu b \bar{t}$ which involve effective 4-fermion couplings \mathcal{G}_{4f} denoted by the blue bulb.

-
- [1] H. Georgi, Nucl. Phys. **B361**, 339 (1991).
 - [2] S. Weinberg, Physica **A96**, 327 (1979).
 - [3] J. Wudka, Int. J. Mod. Phys. **A9**, 2301 (1994), hep-ph/9406205.
 - [4] G. L. Kane, G. A. Ladinsky, and C. P. Yuan, Phys. Rev. **D45**, 124 (1992).
 - [5] D. O. Carlson, E. Malkawi, and C. P. Yuan, Phys. Lett. **B337**, 145 (1994), hep-ph/9405277.
 - [6] E. Malkawi and C. P. Yuan, Phys. Rev. **D50**, 4462 (1994), hep-ph/9405322.
 - [7] D. Espriu and J. Manzano, Phys. Rev. **D65**, 073005 (2002), hep-ph/0107112.
 - [8] D. Espriu and J. Manzano, Phys. Rev. **D66**, 114009 (2002), hep-ph/0209030.
 - [9] C.-R. Chen, F. Larios, and C. P. Yuan, Phys. Lett. **B631**, 126 (2005), hep-ph/0503040.
 - [10] P. Batra and T. M. P. Tait (2006), hep-ph/0606068.
 - [11] J. Alwall et al. (2006), hep-ph/0607115.
 - [12] G. Weiglein et al. (LHC/LC Study Group) (2004), hep-ph/0410364.
 - [13] I. F. Ginzburg, G. L. Kotkin, V. G. Serbo, and V. I. Telnov, Nucl. Instr. Meth. **205**, 47 (1983).
 - [14] E. Boos, A. Pukhov, M. Sachwitz, and H. J. Schreiber, Phys. Lett. **B404**, 119 (1997), hep-ph/9704259.
 - [15] J.-J. Cao, J.-X. Wang, J. M. Yang, B.-L. Young, and X.-m. Zhang, Phys. Rev. **D58**, 094004 (1998), hep-ph/9804343.
 - [16] B. Grzadkowski, Z. Hioki, and M. Szafranski, Phys. Rev. **D58**, 035002 (1998), hep-ph/9712357.
 - [17] S. Weinberg, Phys. Rev. Lett. **43**, 1566 (1979).
 - [18] F. Wilczek and A. Zee, Phys. Rev. Lett. **43**, 1571 (1979).

- [19] H. A. Weldon and A. Zee, Nucl. Phys. **B173**, 269 (1980).
- [20] W. Buchmuller and D. Wyler, Nucl. Phys. **B268**, 621 (1986).
- [21] C. Arzt, M. B. Einhorn, and J. Wudka, Nucl. Phys. **B433**, 41 (1995), hep-ph/9405214.
- [22] F. Larios, M. A. Perez, and C. P. Yuan, Phys. Lett. **B457**, 334 (1999), hep-ph/9903394.
- [23] K. G. Chetyrkin, M. Misiak, and M. Munz, Phys. Lett. **B400**, 206 (1997), hep-ph/9612313.
- [24] G. Burdman, M. C. Gonzalez-Garcia, and S. F. Novaes, Phys. Rev. **D61**, 114016 (2000), hep-ph/9906329.
- [25] G. J. Gounaris, D. T. Papadamou, and F. M. Renard, Z. Phys. **C76**, 333 (1997), hep-ph/9609437.
- [26] S. Eidelman et al. (Particle Data Group), Phys. Lett. **B592**, 1 (2004).
- [27] Q.-H. Cao and C. P. Yuan, Phys. Rev. Lett. **93**, 042001 (2004), hep-ph/0401026.
- [28] M. M. Muhlleitner and P. M. Zerwas (2005), hep-ph/0511339.
- [29] Q.-H. Cao and C. P. Yuan, Phys. Rev. **D71**, 054022 (2005), hep-ph/0408180.
- [30] Q.-H. Cao, R. Schwienhorst, and C. P. Yuan, Phys. Rev. **D71**, 054023 (2005), hep-ph/0409040.
- [31] Q.-H. Cao, R. Schwienhorst, J. A. Benitez, R. Brock, and C. P. Yuan, Phys. Rev. **D72**, 094027 (2005), hep-ph/0504230.
- [32] S. Dawson, Nucl. Phys. **B249**, 42 (1985).
- [33] S. Dawson and S. S. D. Willenbrock, Nucl. Phys. **B284**, 449 (1987).
- [34] C. P. Yuan, Nucl. Phys. **B310**, 1 (1988).
- [35] C.-P. Yuan, Phys. Rev. **D41**, 42 (1990).
- [36] J. C. Pati and A. Salam, Phys. Rev. **D10**, 275 (1974).
- [37] R. N. Mohapatra and J. C. Pati, Phys. Rev. **D11**, 566 (1975).
- [38] R. N. Mohapatra and J. C. Pati, Phys. Rev. **D11**, 2558 (1975).
- [39] G. Senjanovic and R. N. Mohapatra, Phys. Rev. **D12**, 1502 (1975).
- [40] H. Georgi, E. Jenkins, and E. H. Simmons, Nucl. Phys. **B331**, 541 (1990).
- [41] H. Georgi, E. Jenkins, and E. H. Simmons, Phys. Rev. Lett. **62**, 2789 (1989).
- [42] X. Li and E. Ma, Phys. Rev. Lett. **47**, 1788 (1981).
- [43] R. S. Chivukula, E. H. Simmons, and J. Terning, Phys. Rev. **D53**, 5258 (1996), hep-ph/9506427.
- [44] E. Malkawi, T. Tait, and C. P. Yuan, Phys. Lett. **B385**, 304 (1996), hep-ph/9603349.
- [45] D. J. Muller and S. Nandi, Phys. Lett. **B383**, 345 (1996), hep-ph/9602390.

- [46] H.-J. He, T. Tait, and C. P. Yuan, Phys. Rev. **D62**, 011702 (2000), hep-ph/9911266.
- [47] A. Datta, P. J. O'Donnell, Z. H. Lin, X. Zhang, and T. Huang, Phys. Lett. **B483**, 203 (2000), hep-ph/0001059.
- [48] Q.-H. Cao, S.-L. Chen, E. Ma, and G. Rajasekaran, Phys. Rev. **D73**, 015009 (2006), hep-ph/0511151.
- [49] I. Low, JHEP **10**, 067 (2004), hep-ph/0409025.
- [50] J. Hubisz and P. Meade, Phys. Rev. **D71**, 035016 (2005), hep-ph/0411264.
- [51] J. Hubisz, P. Meade, A. Noble, and M. Perelstein, JHEP **01**, 135 (2006), hep-ph/0506042.
- [52] B. Grzadkowski, Z. Hioki, K. Ohkuma, and J. Wudka, Nucl. Phys. **B689**, 108 (2004), hep-ph/0310159.